Invited Paper

Application of the Thermal Line Scanner to Quantify Material Loss Due to Corrosion

K. Elliott Cramer and William P. Winfree
National Aeronautics and Space Administration
Langley Research Center
3 East Taylor St.
Mail Stop 231
Hampton, VA 23681

ABSTRACT

Recent advances in thermal imaging technology have spawned a number of new thermal NDE techniques that provide quantitative information about flaws in aircraft structures. Thermography has a number of advantages as an inspection technique for aircraft. It is a totally noncontacting, nondestructive, imaging technology capable of inspecting a large area in a matter of a few seconds. The development of fast, inexpensive image processors has aided in the attractiveness of thermography as an NDE technique. These image processors have increased the signal to noise ratio of thermography and facilitated significant advances in post-processing. The resulting digital images enable archival records for comparison with later inspections, thus providing a means of monitoring the evolution of damage in a particular structure.

NASA Langley Research Center has developed a thermal NDE technique designed to image and quantitatively characterize the amount of thinning present in metallic materials. The technique involves the movement of a thermal line source across the outer surface of a sample followed by an infrared imager at a fixed distance behind the line source. Images of the material loss due to corrosion are reconstructed from measurements of the induced surface temperature variations. This paper presents a discussion of the development of the thermal imaging system as well as the techniques used to reconstruct images of flaws and to make quantitative thickness measurements. The application of the thermal line source coupled with the analysis technique represents a significant improvement over conventional thermal imaging in the quantification of flaws.

Results of laboratory experiments on specimens with fabricated material loss regions are presented to demonstrate the capabilities of the technique. Additionally, field applications of the technique for both aluminum aircraft structures and steel power plant structures are presented.

Keywords: Infrared, Thermal, NDE, Corrosion

1. INTRODUCTION

The inspection of large aerospace structures, such as aircraft fuselage skins, is a major challenge. The size of these structures limits the usefulness of conventional NDE techniques such as ultrasonics, eddy currents and even conventional thermography. Ultrasonic and eddy current techniques typically involve small area probes that restrict the total inspection area to a small percentage of the fuselage, even if a large scanning mechanism is used. Therefore, NDE inspections typically target known problem areas. Additionally, these techniques are very manpower intensive, imposing a practical limit on the total inspection area covered.

Recent developments have shown the effectiveness of infrared (IR) thermography for the detection of corrosion and disbonds in aircraft structures.[1,2,3] The techniques used typically involve the application of heat and concurrent imaging of the induced temperature change with a stationary IR camera. This offers a rapid method for detecting corrosion and quantifying its extent in single layer structures. While conventional thermography can inspect larger areas (normally 1 m^2 in a matter of a few seconds), one

In *Thermosense XXII*, Ralph B. Dinwiddie, Dennis H. LeMieux, Editors,
Proceedings of SPIE Vol. 4020 (2000) • 0277-786X/00/$15.00

disadvantage of this technique is the expense of the infrared camera. Also, the elevation of the temperature of the entire inspection surface requires a significant amount of power for the infrared heater.

This paper examines an alternate method for thermographically obtaining quantitative corrosion and disbond information in large structures. It is patterned after a technique described by Maldague[4] where a sample moves at a constant velocity past a fixed linear heat source and is observed by an IR imager. Maldague demonstrates that the method is effective for the detection of disbonding in laminated samples.

Results from an alternate implementation of this system where the specimen is stationary and the line heat source and IR camera are translated together at a constant velocity are presented in this paper. This implementation allows the rapid inspection of large structures such as aircraft fuselages. The output of the IR camera is reconstructed to produce an image that represents the induced temperature changes at a fixed distance behind the line heat source.

This method has several distinct advantages over conventional NDE techniques. First, the IR heater is held close to the object of interest, enabling more efficient coupling of the energy into the specimen, reducing the power requirements. This method also enables very high inspection rates (in aluminum, speeds of 25cm/s can easily be achieved). An additional advantage is that a linear array detector can replace the imager, significantly reducing the cost of the system.

This paper presents the results of laboratory measurements on specimens with fabricated thinning that simulates material loss due to corrosion. A theoretical section relates the amount of thinning to the induced temperature change. Examples of this technique applied to actual aircraft samples and structures indicate its capability. Finally, versatility is demonstrated by applying this method to composite structures and materials.

2. EXPERIMENTAL TECHNIQUE

The current implementation of the scanned line source and imager is shown in Figure 1. The IR imager is a commercial radiometer with a cooled 256x256-element InSb (Indium - Antimonide) focal plane array detector. The radiometer's noise equivalent temperature difference (NEDT), cited by the manufacturer, is 0.025°C when operating the detector in the 3 to 5 micrometer wavelength range. The radiometer produces images at both 30 frames per second output (video frame rate, in an RS170 format compatible with standard video equipment) and 60 frames per second output in a 12-bit, RS422 digital format. External optics, consisting of a wide-angle lens, using germanium optical elements, was used to increase the system field-of-view by a factor of approximately two. The expanded field-of-view of this lens is 22° in both the horizontal and vertical directions. The future implementation of a linear array of detectors, in place of the IR camera, would significantly reduce the cost of the system without impacting flaw detectability.

Focusing a commercially available 3000-watt quartz lamp, with an elliptical reflector behind the quartz tube, approximates a line of heat. The heat source and the IR imager are attached to a commercial linear scanning bridge. Quantitative time based analysis requires synchronization between the IR imager, the heat source and the scanning table. This synchronization is achieved by computer control of the application of heat, motion of the scanning table and data acquisition. The computer can provide any scanning speed rate up to 30.5 cm/sec, the mechanical limits of the scanning table. For all cases presented in this paper the maximum surface temperature change of the specimen above ambient was less than 10°C.

For low emissivity surfaces, it is necessary to enhance the emissivity by coating the surface. Paint is typically a good emissivity coating. If the specimen is painted, regardless of color, no additional surface coating is necessary. Unpainted metallic samples require the addition of an emissivity enhancing coating. For the results presented here, the metallic samples were treated with either a water washable, nontoxic paint or a flat black aerosol lacquer to increase the emissivity.

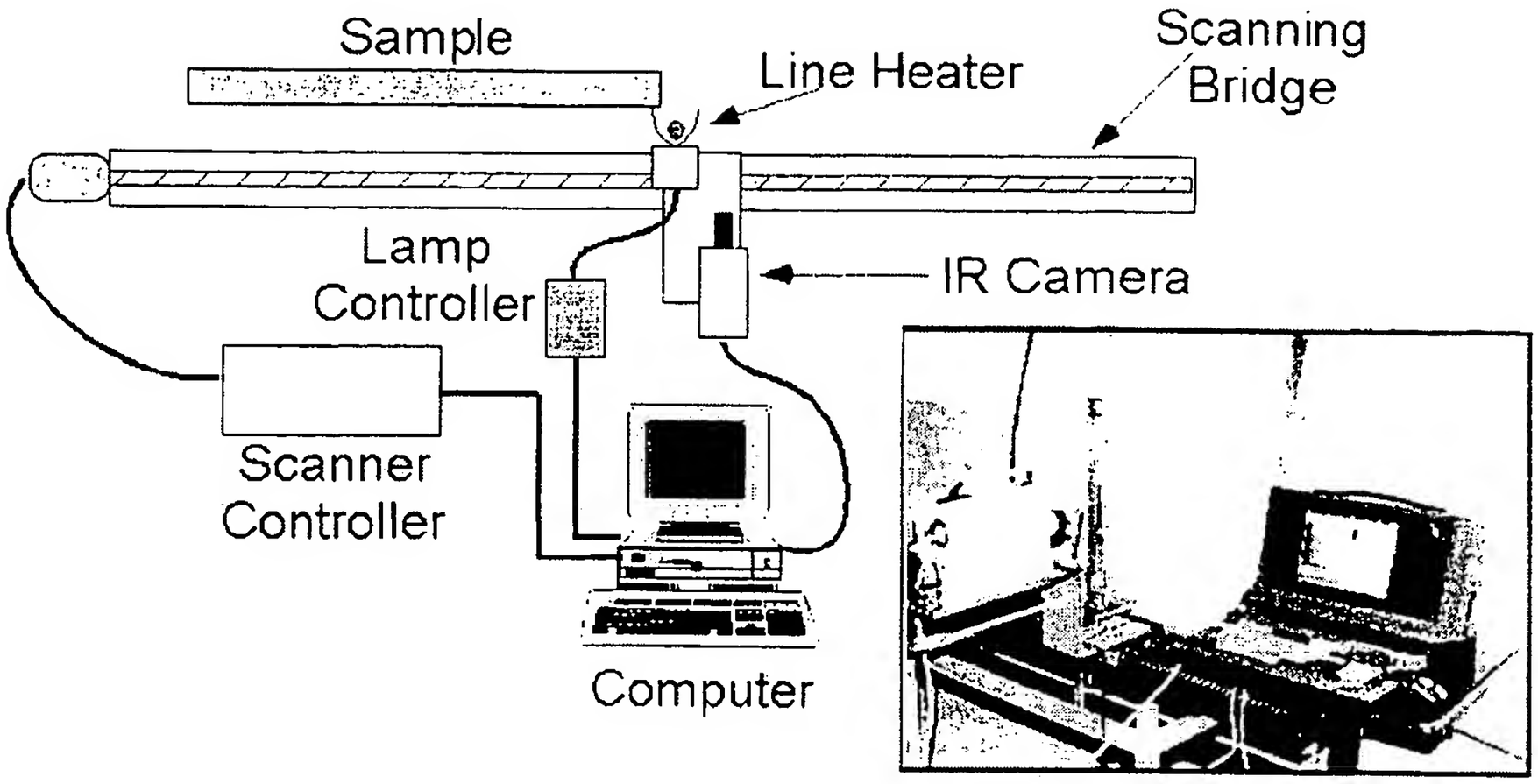

Figure 1 – Schematic and photograph of experimental setup used to implement moving line source technique.

The digital data from the radiometer was acquired and stored at rates up to 60 frames-per-second using a real-time image processor board in the control computer. The image processor board has 256 megabytes of image memory available for storage and is capable of real-time floating point processing of the incoming data. The imaging camera moved with the heat source, enabling data acquisition at a fixed distance from the source. From a set of acquired images, a single image was then reconstructed that represents the induced temperature change at a fixed distance from the heat source. The reconstructed image is typically 256 pixels high and up to 1200 pixels wide (depending on the physical length of the sample, the speed of the scanner and the image acquisition rate). This reconstruction is currently done either in real-time by the image processor, or as post-processing analysis of the data. All of the data presented in the remainder of the paper (unless otherwise noted) were reconstructed in this manner.

3. ANALYTICAL SOLUTION FOR MOVING LINEAR HEAT SOURCE

Assuming a medium of thickness L, with an infinitely long line source moving along the surface at a fixed velocity (v) and from a frame of reference moving with and centered on the heat source, It has been shown that the far field temperature distribution is given by[5]:

$$T(x,z)=\frac{q}{Lv\rho c}\left[e^{-v\frac{(x+|x|)}{2\kappa}}+2v\sum_{n=1}^{\infty}\mathrm{Cos}\left(\frac{n\pi z}{L}\right)\frac{e^{-\frac{vx+|x|\sqrt{(2n\pi\kappa/L)^2+v^2}}{2\kappa}}}{\sqrt{(2n\pi\kappa/L)^2+v^2}}\right] \quad (1)$$

where q is the input heat flux, ρ is the density, c the specific heat and κ the thermal diffusivity of the material.

Examination of Equation 1 indicates that when the summation is approximately equal to zero, the temperature becomes a constant, q/(Lvρc), if x is negative. For lower velocities ($v < 2\kappa/L$), the condition necessary for the summation to be approximately zero is

$$x < \frac{2\kappa}{v - \sqrt{(2\pi\kappa/L)^2 + v^2}} \approx \frac{L}{\pi}. \tag{2}$$

At higher velocities ($v > 2\kappa/L$), the condition where the summation is zero is approximated when the distance behind the line source is equal to the thickness of the plate. When this occurs, the temperature in the far field behind the source is given by

$$T \approx \frac{q}{Lv\rho c}. \tag{3}$$

It can be seen from equation (3) that the observed temperature of the surface is inversely proportional to the thickness of the material and can thus be used directly to measure the changes in thickness as long as the above condition is satisfied.

4. EXPERIMENTAL MEASUREMENTS OF STEEL SAMPLES

Figure 2 shows a diagram of a low carbon steel specimen fabricated to confirm Equation (3). The specimen was 121.9 cm in length, 45.7 cm in width and had a nominal thickness of 0.635 cm. A 10.2 cm wide region spanning the length of the specimen was reduced in thickness to 0.318 cm and three regions (25.4 cm in length and 5.1 cm in width separated by 12.7 cm) centered on the panel were reduced in thickness to 0.508 cm, 0.445 cm and 0.381 cm respectively.

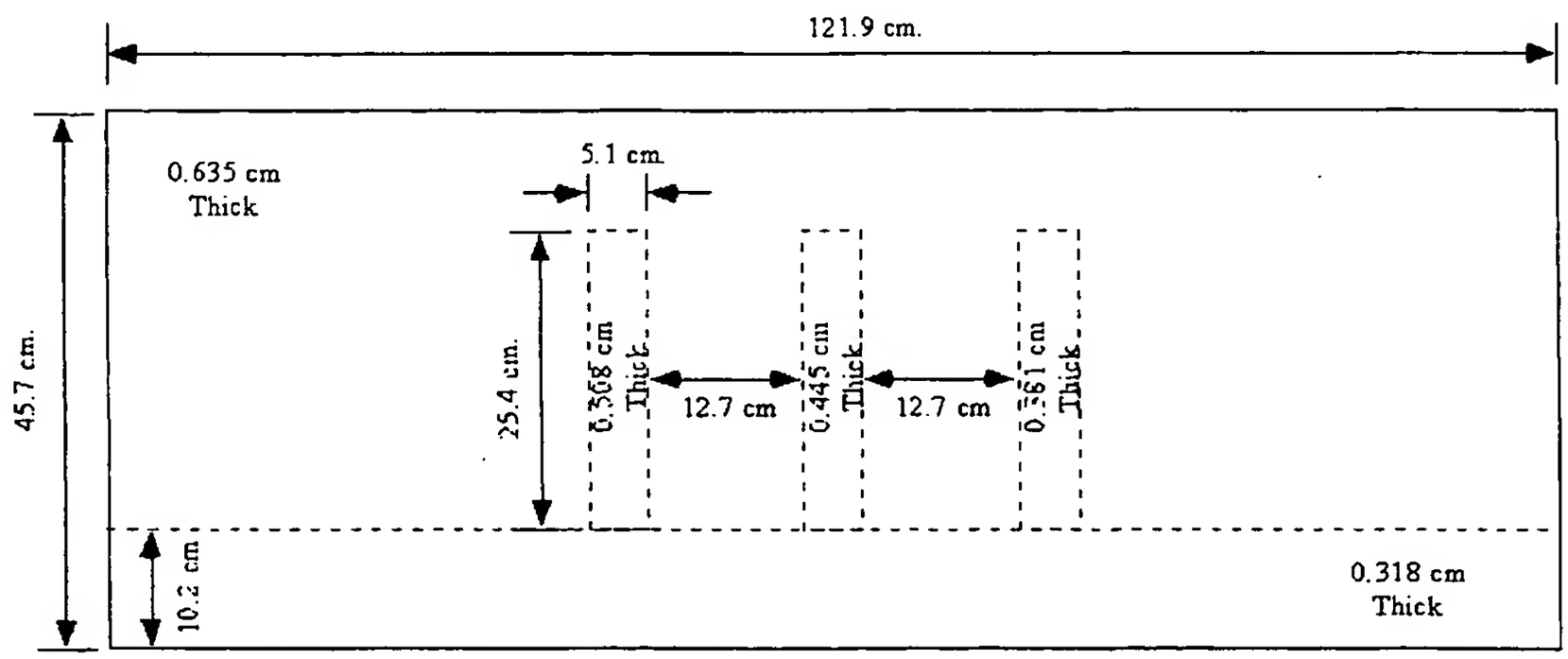

Figure 2 – Steel specimen with three sets of material loss regions, 0.508 cm, 0.455 cm and 0.381 cm deep respectively, centered on the panel and separated by 12.7 cm. Each region is 5.1 cm wide and 25.4 cm long. A region 10.2 cm wide and spanning the length of the specimen was reduced in thickness to 0.318 cm.

Data was acquired on the specimen while moving the heat source and imager across the surface at a velocity of 3.81cm/s ($2\kappa/L$ in this case is approximately 0.38 cm/s). An image acquisition rate of 30 frames per second was used. Figure 3 shows an image and surface temperature profile obtained for a line of detectors 3.5 cm behind the line of heat. The relationship between the scanning speed and the separation distance between the line of heat and the detectors has been addressed in previous work[5]. It is difficult to

apply Equation (3) directly do the data since in practice q is complicated to measure and ρ and c are many times unknown as well. Therefore the 0.635 cm thick region across the top of the specimen and the 0.318 cm thick region at the bottom were used to perform a linear regression on the data in the center of the panel to calculate specimen thickness. The results of this data reduction, averaged over the area of the three interior material loss regions, and compared to the actual panel thickness is shown in Figure 4. It can be seen that the while the data agrees well in some areas, in other areas the calculated thickness deviates from the actual by as much as 4.8%. This variation may be due to warping of the specimen that occurred during fabrication. This warping made it difficult to keep the line heat source parallel to the specimen during the entire length of the data collection scan.

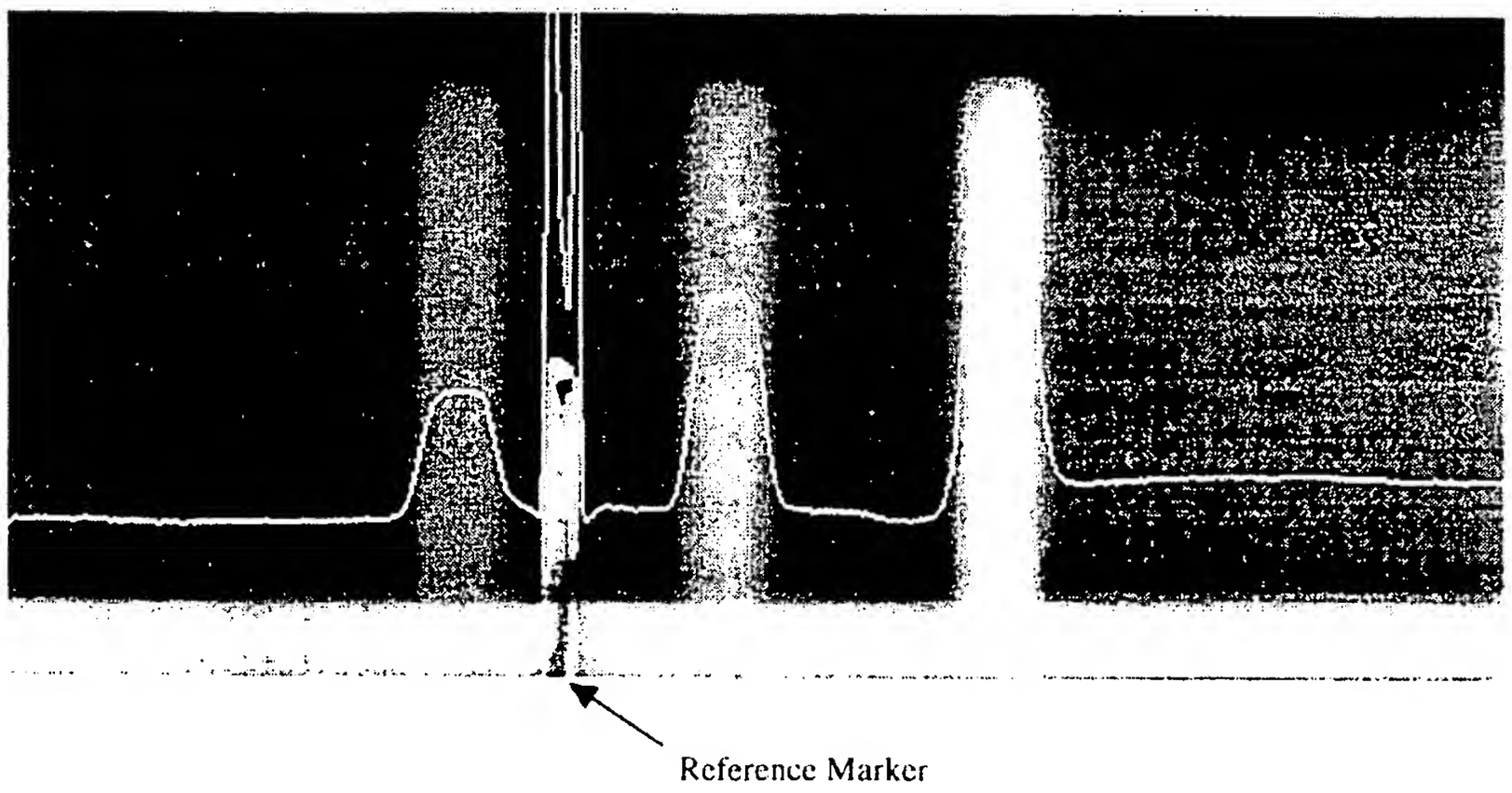

Figure 3 -- Thermal line scanner image and surface temperature profile for steel thickness specimen. A reflective tape reference mark was placed on the surface of the sample before scanning.

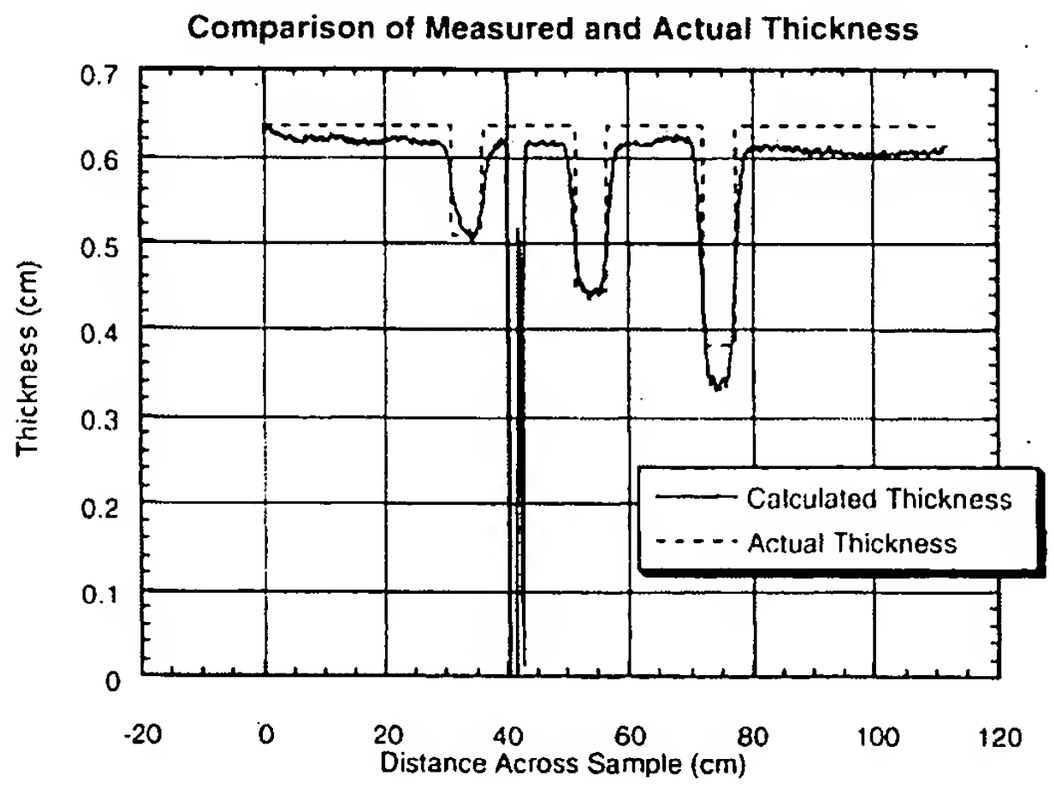

Figure 4 – Comparison of the actual thickness of the steel specimen with the thickness calculated from the thermal line scanner temperature data.

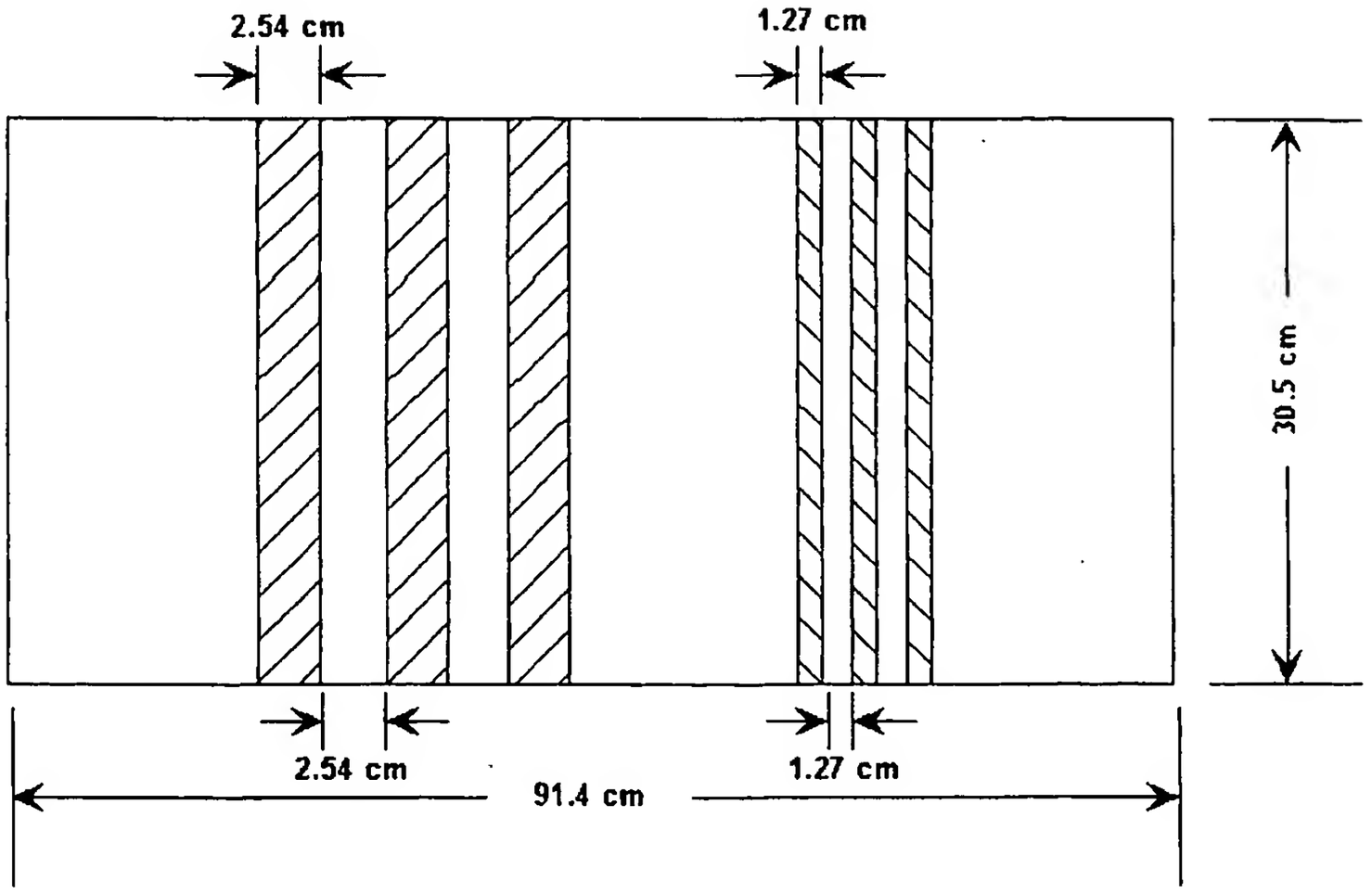

Figure 5 – Steel sample with two sets of 0.12cm deep material loss regions. The first set being 2.54cm wide with a 2.54cm separation and the second being 1.27cm wide with a 1.27cm separation.

To investigate the relationship between the measured surface temperature and the size of thickness variations, a specimen was created with multiple regions of material loss as shown in Figure 5. The specimen is 91.4 cm long, 30.5 cm wide and has a nominal thickness of 0.30 cm. The specimen has two sets of grooves, both 0.12 cm deep. The grooves in the first set are 2.54 cm wide with a spacing of 2.54 cm between grooves. The second set of grooves are 1.27 cm wide and have spacing of 1.27 cm. Steel was chosen as the material for this sample to allow the effects of variations in speed to be investigated over the reasonably small velocity range of the scanning table. These effects have been reported previously[5].

Data was acquired on the specimen while moving the heat source and imager across the surface at a velocity of 7.62cm/s. An image acquisition rate of 60 frames per second was used. Figure 6 shows an image obtained for a line of detectors 3.25cm behind the line of heat. In this case a simple linear regression of the data results in an under estimation of the thickness of the narrower set of grooves.

From these results it can be seen that quantitative analysis of the amount of material loss in a panel using this system can be difficult. Not only is the measured temperature dependent on the speed of the moving line, but also on the separation distance between the lamp and the imager and then finally on the size of the defect present[5]. It has been shown that a significant improvement in the quantitative results of this technique can be achieved by a nonlinear mapping of the inverse of the temperature to thickness using neural networks[6,7].

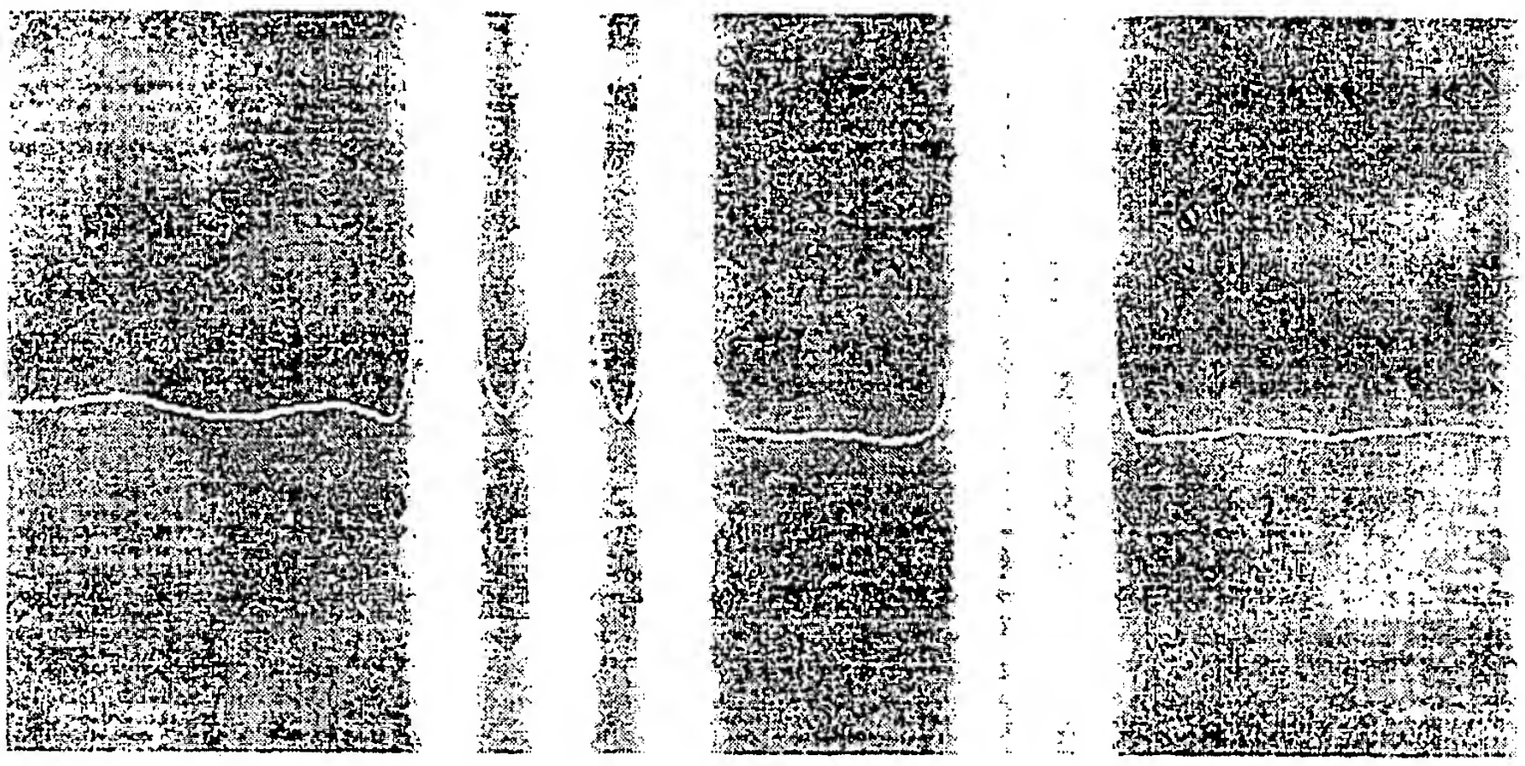

Figure 6 – Thermal line scanner image and surface temperature profile for steel resolution sample showing the effect of defect size on surface temperature profile.

5. AIRCRAFT FUSELAGE SAMPLES AND STRUCTURES

Of particular interest is the applicability of this technique to aircraft structures. A sample was cut from a commercial aircraft that had been retired from service. The sample is 101.6 cm in width and 96.5 cm in height. It consists of two 2024-T3-aluminum skins. The upper skin has a thickness of 1.60 mm and the lower skin has a thickness of 1.02 mm. The skins are joined in a lap type joint were no bonding material was used but the joint was fastened by 3 rows of rivets. Since previous inspections of this sample, using conventional IR thermography, indicated that there was no corrosion present in the lap joint, a 7.6 cm square region adjacent to the lap joint was electrochemically etched to produce a material loss of approximately 15%. Figure 7 shows the results for this sample. There is a clear distinction between the temperature in the thicker upper skin, the thinner lower skin and the material loss region. Additionally, the absence of adhesive bonding material in the lap joint is observable in the results since the amplitude of the thermal response over the lap joint is the same as in the upper skin.

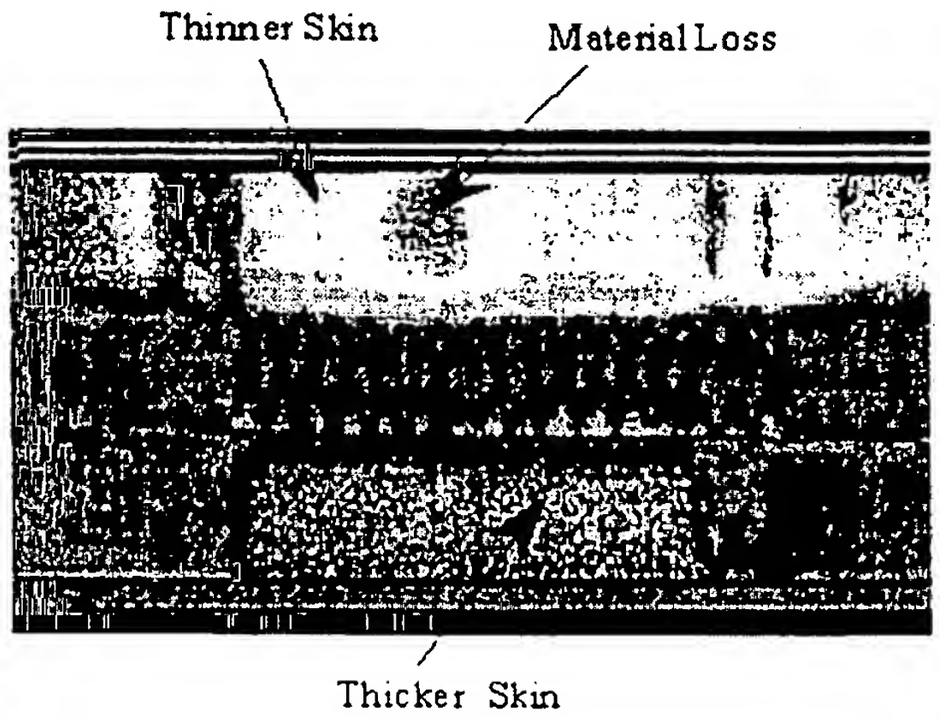

Figure 7 – Results for actual aircraft sample with both no bonding in lap joint and material loss in skin immediately above joint. Differences in skin thickness can also be observed.

To further investigate the applicability of this technique to actual aircraft, an inspection was performed at the Airworthiness Assurance Nondestructive Inspection Validation Center (AANC) operated by Sandia National Laboratories in Albuquerque, N.M. for the FAA William J. Hughes Technical Center, Atlantic City, N.J. The inspections were performed on the Boeing 737-222 aircraft test-bed. Figure 8 is a composite thermal image that resulted from inspecting 330 cm of lapjoint, aft of the left wing. An inspection speed of 12.7 cm/s, based on the thickness and thermal diffusivity of the fuselage material, was chosen for the apparatus described above. Since the scan length is limited in the current setup to 150 cm, three scans were use to produce the image in Figure 8. Total time for the inspection, not including repositioning the scanning apparatus, was 30 seconds. While no corrosion was found in this inspection, indications of disbonding are visible in the image.

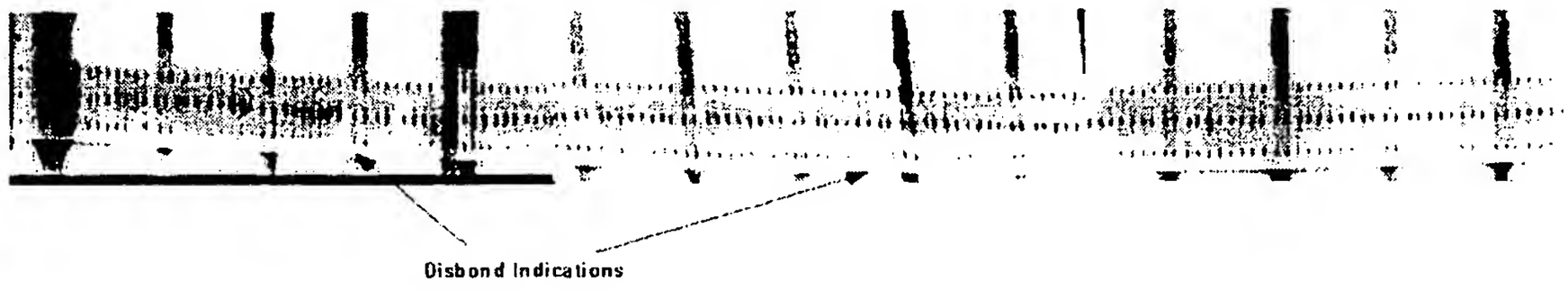

Figure 8 – Results for actual aircraft inspection showing some indications of lapjoint disbonding.

6. OTHER APPLICATONS

The thermal line scanner has been shown to be well suited to thickness measurements in homogeneous materials, it also has many additional applications. For example Figure 9 shows the results of scanning a composite honeycomb structure at 5 cm/s. The specimen consisted of graphite-epoxy face sheets enclosing an aluminum honeycomb core. The overall sample dimensions are 47.6 cm in length, 30.5 cm in width and 2.5 cm thick. Entrapped water can be seen in the image as large low temperature (dark) areas. Another example is seen in Figure 10, which shows the results of scanning a graphite epoxy composite fatigue specimen at 3.8 cm/s. The specimen is 82.55 cm in length, 30.48 cm in width and 0.22 cm thick over the test region with grip ends thickened to 0.62 cm. This sample was fatigued in a material test frame until failure. The resulting fatigue crack is visible in the resulting thermal line image.

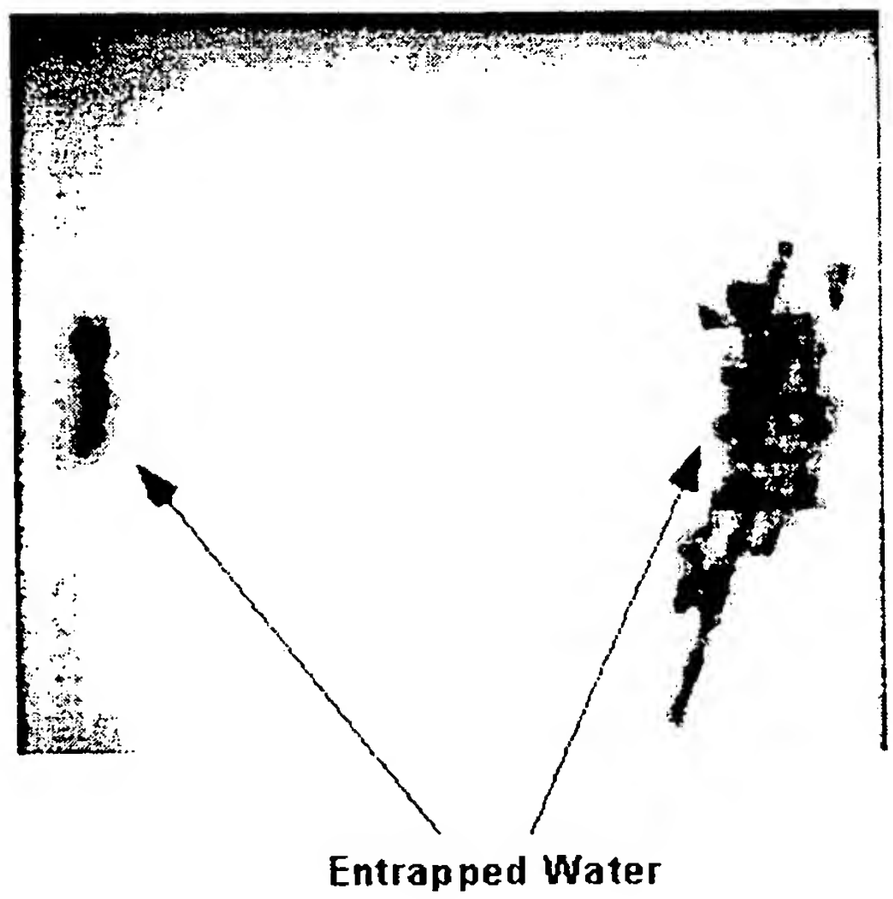

Figure 9 – Thermal line scan image of water entrapped in the honeycomb structure behind a graphite epoxy skin.

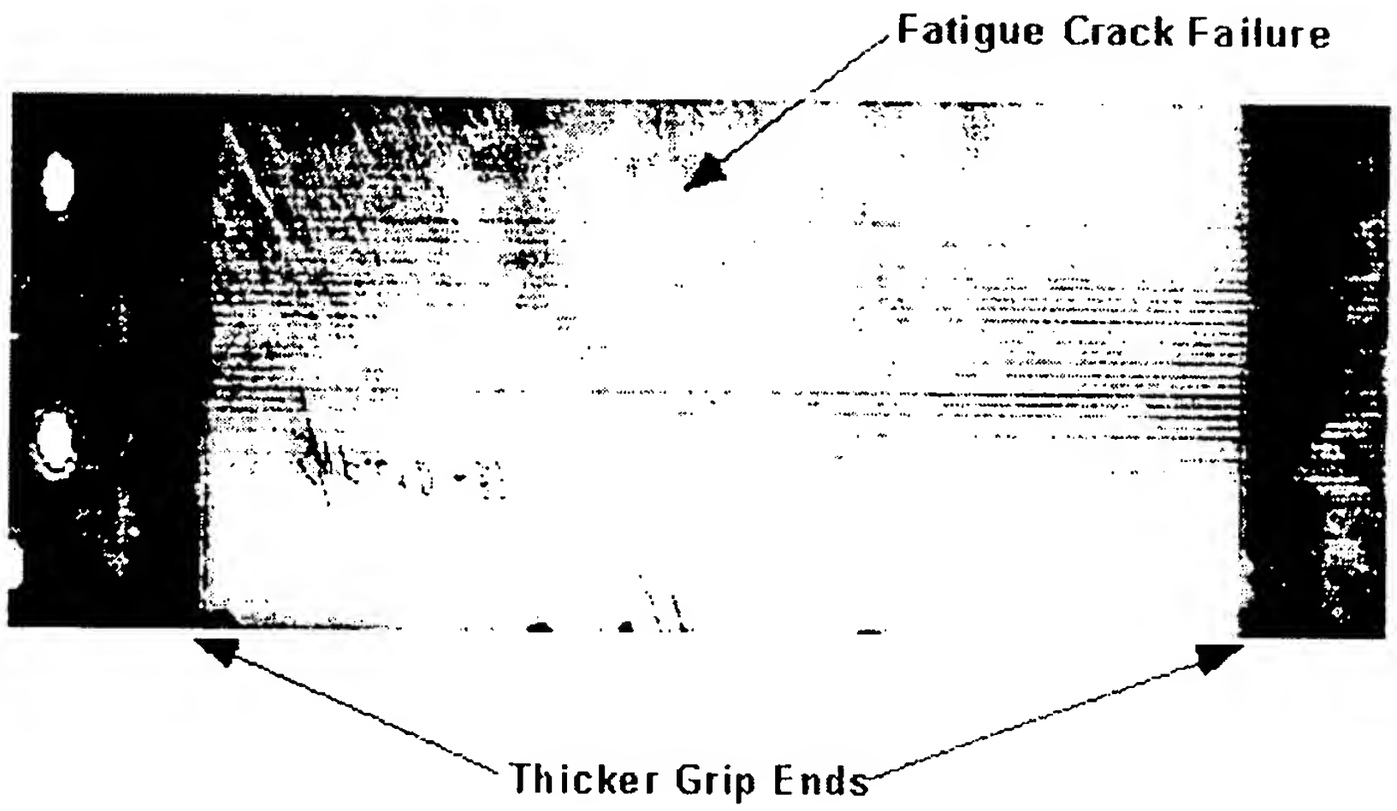

Figure 10 – Thermal line scan image of graphite epoxy composite fatigue test specimen. Changes in thickness as well as fatigue crack failure can be seen in the image.

7. CONCLUSIONS

A noncontacting thermal NDE technique has been developed which employs a moving line heat source and is capable of imaging defects in thin aluminum structures such as aircraft lap joints. This technique has been demonstrated to effectively detect thinning in thin steel laboratory samples. A steady state solution for the induced thermal change in the plate has been developed that indicates that the induced temperature change is inversely proportional to the thickness of the material at an observation point more than one thickness of the plate behind the linear source. This information has been used, with good results, to reconstruct the back surface profile of single layer plates containing material loss regions[6,7]. The experimental results are in good agreement with theoretical results. Examples of the application of the technique to aircraft structures have yielded promising qualitative results.

In the future, additional analysis methods that take advantage of the data acquired at multiple observation points should significantly improve the results and allow for quantitative analysis of the structure. One such analysis method could involve reconstructing a series of images from the data acquired, each image at a different distance from the heat source. These images can then be treated as a time series and variations in the heat propagation rates can be explored by a number of time-based analysis methods. This analysis method has the potential to produce images of the complete thermal diffusivity tensor of the specimen. Thermal diffusivity imaging has proven to be quite valuable in detecting and characterizing defects in composite materials and structures[8,9]. Practical application of this technique requires a more fieldable scanning configuration. A linear robotic scanner that could efficiently transport the heat source and imager over large areas of an aircraft has great potential.

8. REFERENCES

1. L.D. Favro, T. Ahmed, X. Han, L. Wang, X. Wang, P.K. Kuo and R.L. Thomas, *Review of Progress in QNDE*, Vol. 15, eds. D.O. Thompson and D.E. Chimenti (Plenum, New York, 1996), p. 1747.
2. N. K. Del Grande, P.F. Durbin and D.E. Perkins, *Review of Progress in QNDE*, Vol. 12, eds. D.O. Thompson and D.E. Chimenti (Plenum, New York, 1993), p. 465.
3. K.E. Cramer, P.A. Howell and H.I. Syed, *Proceedings SPIE - Thermosense XVII*, Vol. 2473, ed. S. A. Semanovich (SPIE,Bellingham,1995), p. 226.
4. X.P.V. Maldague, *Nondestructive Evaluation Of Materials By Infrared Thermography*, (Springer-Verlag, London, 1993).
5. K.E. Cramer and W.P. Winfree, *Proceedings SPIE - Thermosense XX* , Vol. 3361, eds. J.R. Snell, Jr. and R.N. Wurzbach (SPIE,Bellingham,1998), p. 291.
6. W.P. Winfree and K.E. Cramer, *Review of Progress in QNDE,* to be published.
7. W.P. Winfree and K.E. Cramer, *Proceedings SPIE – Thermosense XXII,* to be published.
8. C.S. Welch, D.M.Heath, W.P.Winfree, *J. Appl. Phys.*, **61**, pp. 895-898, 1987.
9. K.E. Cramer, W.P. Winfree, E.R. Generazio, R. Bhatt and D.S. Fox, *Review of Progress in QNDE*, Vol. 12, eds. D.O. Thompson and D.E. Chimenti (Plenum, New York, 1993), p. 1305.